Journal of Molecular Structure 1289 (2023) 135866

Contents lists available at ScienceDirect

Journal of Molecular Structure

journal homepage: www.elsevier.com/locate/molstr

Inclusion complexation of biphenyl-3,3′,4,4′-tetraamine and 4,4′-diaminobiphenyl-3,3′-diol with β-cyclodextrin for antibacterial activity

Kumaraswamy Paramasivaganesh [a,b,1], Vimalasruthi Narayanan [a], Vigneshkumar Ganesan [a], Esakkimuthu shanmugasundram [a], Rajaram Rajamohan [c,1], Yong Rok Lee [c,*], Stalin Thambusamy [a,*]

[a] Department of Industrial Chemistry, Alagappa University, Karaikudi 630 003, Tamil Nadu, India
[b] Department of Chemistry, Arumugam Pillai Seethai Ammal College, Thiruppuvur 630 211, Tamil Nadu, India
[c] Organic Materials Synthesis Laboratory, School of Chemical Engineering, Yeungnam University, Gyeongsan 38541, Republic of Korea

ARTICLE INFO

Keywords:
Biphenyl compounds
β-Cyclodextrin
Inclusion complexes
Binding constant
Antibacterial activity

ABSTRACT

Inclusion complex (IC) of β-cyclodextrin (β-CD) with biphenyl-3,3′,4,4′-tetraamine (BPT), and 4,4′-diaminobiphenyl-3,3′-diol (DABD) are prepared and investigated in both solution and solid state. The effect of β-CD on the enhancement of solubility, stability, and antibacterial activity of poorly water-soluble BPT and DABD. Ultraviolet (UV), Fluorescence (FL), and Cyclic Voltammetric (CV) methods are particularly useful for determining stoichiometric ratios and binding constants in liquids. The prepared solid-phase ICs between host and guest are confirmed by powder XRD, SEM, DTA, FT-IR, and ^{1}HNMR results. These results revealed that both BPT and DABD molecules formed ICs with β-CD with the stoichiometric ratio of 1:1.In this case, structurally confirmed ICs are required for investigating antibacterial activity, and their biological properties are as expected. It is widely acknowledged that these ICs recommended to the pharmaceutical and food industry due to their effective solubility, stability, and antibacterial activity.

1. Introduction

Biological activity is an important term, that describes the interaction of chemicals with the human body [1]. The biological activity is derived from the chemical structure, its physicochemical properties, bioavailability unit, and mode of treatment. Furthermore, the majority of chemical substances exhibit a wide range of biological action [2]. While some of them are beneficial in treating particular disorders, others may be poisonous and have several negative side effects. Additional research also revealed that polyphenol [3] and amine-type compounds [4] are available for the treatment of fungal infection compounds and their derivatives possess important biological properties, including those related to antiviral, antimalarial, anticancer, anti-tumor, anti--mycobacterial, anti-convulsant, anti-analgesic, anti-inflammatory, anti-platelet, and anti-tumoral activities [5–7]. The biphenyl-3,3′,4,4′-tetraamine (BPT), and 4,4′-diamino biphenyl-3,3′-diol (DABD) (Scheme 1) both are typical amino functional organic compounds so, they can be applied in various chemical and biological industries. Unfortunately, it's low water solubility and chemical stability so improve their solubility purpose, focused on supramolecular chemistry.

A more important thrust research area in photochemistry is the origin of supramolecular chemistry based on molecular recognition and molecular interactions, which are the host molecules recognizing their guest molecules. In the inclusion complexation process, Zeolites [8,9], Octa acids [10–12], Cyclodextrins [13,14], Cucurbiturils [15,16] Calixarene [17], Crown Ethers [18], and Cyclophanes are more important hosts. α-cyclodextrin (α-CD), β-cyclodextrin (β-CD), and γ-cyclodextrin (γ-CD), a family of cyclic oligosaccharides, have been implicated in host-guest ICs via hydrophobic interactions and allow the formation of ICs with organic and drug molecules [19–23]. β-CD, in particular, has made a greater contribution to their inclusion complexation in research development [24–27]. Because β-CD is connected to seven glucose subunits via 1,4 glycosidic bonds (Scheme 1), it is both hydrophilic and hydrophobic. This property primarily influences the formation of organic ICs (Scheme 1) or partial ICs with larger molecules. These types of inclusion complexation can improve the physicochemical properties

* Corresponding authors.
E-mail addresses: yrlee@yu.ac.kr (Y.R. Lee), stalin.t@alagappauniversity.ac.in (S. Thambusamy).
[1] Contributed equally to this work

https://doi.org/10.1016/j.molstruc.2023.135866
Received 21 March 2023; Received in revised form 19 May 2023; Accepted 24 May 2023
Available online 26 May 2023

such as solubility, stability, and, more importantly, the antibacterial activity of the IC [28–30]. The experimental and theoretical approaches also contributed to the proposed mechanism for the ICs, which is critical for improving dissolution and phase solubility in pharmaceutical applications [31–37]. One of the future investigations involving solid inclusion complexes in supramolecular chemistry is to analyze or regulate the temperature of phase-change, release, and breakdown of the guest. Not only does it have practical relevance for β-CD inclusion complexes for cyclodextrin chemistry, but it is also one of the most significant and fascinating topics at the moment. Because it has consequences for how we should interpret the distinctions in the intermolecular interactions among free, complex, and survivable molecules, as well as for applications in medicine, food additives, cosmetics, and biological products. Recent investigations have published a lot of papers in the field of inclusion complexes with electrospun nanofibers [38–42].

In addition to ICs, CDs form head-to-tail dimers [43]. Furthermore, the encapsulation of CDs in liposomes has a promising activity against all Gram-negative bacteria [44] and the Cucurbit[6]uril bridged Cyclodextrin dimer mediated stable ICs with intramolecular fluorescence resonance energy transfer (IFRET) behavior [45]. There are a number of reports in the literature that are specific to understanding the ICs, but none for the following BPT and DABD with β-CD. The incorporation of β-CD into their compound enhances the solubility and thermal stability of BPT and DABD. This prompted us to investigate the complexation of these molecules in the liquid and solid states. Electronic spectroscopy and the cyclic voltammogram are used to analyze the binding ability of the host and guest molecules in the liquid state of ICs. For the preparation of ICs as solids, a number of techniques have been developed, including co-precipitation, freeze-drying, kneading, and solid-state grinding. Additionally, the ICs would be proven as active materials for antibacterial activity.

2. Materials and methods

2.1. Instruments

The UV–visible spectra for the absorption measurements are made with a Shimadzu UV-2401PC double-beam spectrophotometer with wavelength ranges between 800.0 and 200.0 nm and a scan speed is about 400.0 min^{-1}. Fluorescence measurements are made by the Jasco FP-550 fluorescence spectrophotometer. The instrument is conventional to make a measurement at every 0.5 nm interval in the particular wavelength range. A standard quartz cuvette with a light path of 1.0 cm is generally used for the complete measurements. The pH values are measured on Elico pH meter LI-120.FT-IR spectra are made using Nicolet 380 Thermo Electron Corporation Spectrophotometer using KBr pellets and the ranges between 4000.0 and 400.0 cm^{-1}.^{1}H NMR spectra are taken with BRUKER-NMR 500 MHz. The solutions for ^{1}H NMR are prepared by dissolving analytes and their ICs in DMSO-d_6 solvent to obtain the final concentration of 20 mM. Powder X-ray diffraction spectra are taken withXPert PRO PANalytical diffractometer (2 Theta:0.001; Minimum step size Omega: 0.001). Thermal analysis is measured in SDT Q600 V8.0 Build 95. The surface morphology of the samples is made with an SEM instrument with Hitachi S 3000 H.

2.2. Chemicals

β-CD is obtained from Himedia Chemical Company and used as such. Biphenyl-3,3′,4,4′-tetraamine (BPT), and 4,4′-diaminobiphenyl-3,3′-diol (DABD) are obtained from Alfa-Aesar, Shore Road, Heysham,

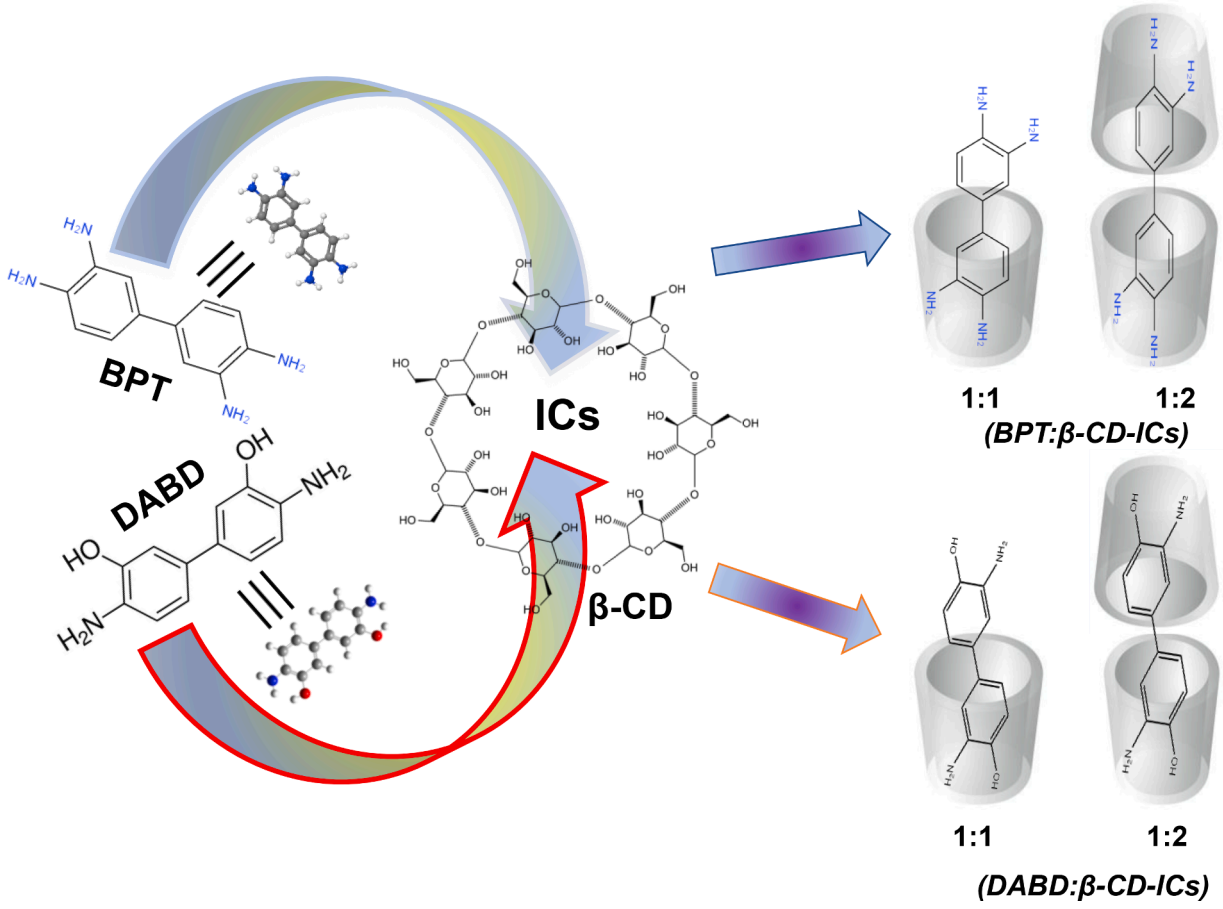

Scheme 1. Structures of BPT, DABD, β-CD, and schematic representation of the ICs.

England. Throughout our research, we used ultra-pure water.

2.3. Preparation of solutions of β-CD and biphenyl compounds

The highest stock solution of β-CD (12×10^{-3} M) and guest 2.0 × 10^{-3} M, are prepared using Millipore water and ethanol, respectively. 0.2 ml of both the guest BPT and DABD are accurately added into 10.0 ml volumetric flasks and adjusted to the concentration of β-CD solutions of 0, 2.0, 4.0, 6.0, 8.0, 10.0, and 12.0 M. To obtain a homogeneous solution, all flasks are thoroughly shaken. As a result, the final concentration of BPT and DABD in each flask is approximately 2×10^{-5} M. At room temperature, all absorption and fluorescence spectra are recorded. The absorbance and emission information were completely observed with the assistance of the Jasco V-670 Spectrophotometer within the range extending 400 to 800 nm with the time 120 s per one spectral measurement.

2.4. Determination of stoichiometric ratio and binding constant

The BH equation [34] yields the ICs' stoichiometric ratio and binding constant, which are related to changes in absorbance and fluorescence intensity. Even though the changes in absorbance or emission intensity of the guest molecules are very small after the addition of β-CD, the values are obtained with the help of BH equations. The 1:1 ICs' Eq. (1) is given below.

$$\frac{1}{(A-A_0)} = \frac{1}{(A'-A_0)} + \frac{1}{K(A'-A_0)(\beta-CD)} \cdots\cdots\cdots \quad (1)$$

In this equation, A_0 indicated the intensity of the guest's absorbance in the absence of β-CD, A indicated the absorbance with a specific concentration of β-CD, A′ indicated the absorbance at the maximum concentration of β-CD used, and "K" is the binding constant. The plot of $\frac{1}{(A-A_0)}$ *Vs* $\frac{1}{[\beta-CD]}$ for the 1:1 ICs shows linearity and the K is calculated as per Eq. (2).

$$K = \frac{1}{slope\ (A'-A_0)} \cdots\cdots\cdots \quad (2)$$

For fluorescence spectra, the BH Eq. (3) for 1:1 ICs is given by Eq. (3)

$$\frac{1}{(I-I_0)} = \frac{1}{(I'-I_0)} + \frac{1}{K(I'-I_0)[\beta-CD]} \cdots\cdots\cdots \quad (3)$$

In the above equations, I_0 represents the emission intensity of the guest without the addition of β-CD, I represents the emission intensity with a specific concentration of β-CD, I' represents the emission intensity at the highest concentration of β-CD used for the study, and K represents the binding constant. Linearity is obtained in the $\frac{1}{(I-I_0)}$ *Vs* $\frac{1}{[\beta-CD]}$ plot for the 1:1 complex (Eq. (3)). Using Eq. (4), the binding constant K is calculated by the use of Eq. (4).

$$K = \frac{1}{slope(I'-I_0)} \cdots\cdots \quad (4)$$

2.5. Preparation of ICs in solid state

One gram of β-CD is accurately weighed and placed in a 250 mL conical flask, to which 30 mL of Millipore water is added and thoroughly stirred. The equimolar weight of biphenyl derivatives (guest, BPT & DABD) is then placed in a 100 mL beaker, and 20 mL ethanol is added and allowed to stir over an electromagnetic stirrer. The guest solutions are gradually poured into the aqueous solution of β-CD. The above-mixed solutions are continuously stirred at room temperature for 48 h. The reaction mixture is refrigerated for about 48 h. At this point, a white precipitate of BPT and DABD with β-CD has formed. The precipitate is washed with Millipore water after being filtered by a G4 crucible. The precipitate is placed in a Petri dish and spread thinly over the surface before being dried in an oven at 50 °C for 12 h. The solid ICs are obtained after drying in the oven. The ICs are also prepared physically, with the β-CD and guest molecules ground for two hours without any solvent in a mortar and pestle, and the finely divided particles of the complex are taken for analysis. Similarly, for the kneading method, we ground the guest and host in a mortar and pestle with a small amount of solvent for two hours until they formed a paste and dried at room temperature. The ICs are employed in the analysis. These are the standard techniques for characterizing the ICs of biphenyl derivatives with the β-CDincludes FT-IR, ^{1}H NMR, powder XRD, DSC, and SEM analysis.

2.6. Preparation of stock solutions for antibacterial activity studies

In all the cell lines procured from ATCC, the procured cells were inoculated in a 10 ml test tube and incubated in an orbital incubator shaker overnight at 37 °C (120 rpm). The nutrient broth was used for culturing different microbes. The viability of the cells is checked by further plating and found to be viable. The antibacterial activity of the samples is made using a stock solution of the ICs (2.0×10^{-4} M) which was tested against gram-positive bacteria (*s. aureus*) and gram-negative bacteria (*E. coli*) using the *in-vitro* disc agar diffusion method. The bacteria growth was done for 24 h and incubated at RT.

3. Result and discussion

3.1. Concentration-dependent UV–visible and fluorescence spectral studies

The absorption maxima and relevant spectra of BPT and DABD (2×10^{-4} M) in pH 7.0 solutions containing different concentrations (0, 2.0, 4.0, 6.0, 8.0, 10.0, and 12.0 M) of β-CD are shown in Fig. 1 and the data is consolidated in Table 1. BPT and DABD exist in a neutral form at pH 7. In the absorption spectra of both molecules, no isosbestic point is observed due to no covalent bond being possible between the β-CD and BPT or DABD molecules. In the pristine BPT exhibit, the two absorbance bands such as 315 and 229 nm owing to π-π* and *n*-π* transition. In the presence of β-CD, the BPT exhibits a significant blue shift in both the longer wavelength (315.0 to 302.0 nm) and shorter wavelength (229.0 to 231.0 nm) may be possible to hydrogen bonding between the BPT containing an electronegative atom of nitrogen and β-CD hydroxyl group. Moreover, shifts at higher wavelengths are blue-shifted, while the shifts at lower wavelengths are red-shifted, demonstrating the molecule's inclusion behavior, and the increase in absorbance at the wavelengths is revealed the guest molecules entrapped in the host molecule. When the concentrations of β-CD exceed 12.0×10^{-3} M , the absorbance and fluorescence intensities remain unaltered. It is worth noting that the DABD molecule exhibits a remarkable red shift, and the intensity is greatly increased by the gradual addition of β-CD concentration evident for the formation of ICs.

The enhanced solubility of BPT and DABD molecules due to the hydrophobic interaction with β-CD has been attributed to this behavior. These findings suggested that BPT and DABD molecules are included in the cavity of β-CD and formed ICs. In the UV spectra of DABD and BPT, the peaks broaden as the concentration of β-CD increases, and the peaks almost disappear at high concentrations; these peaks correspond to the formation of ICs with 1:1 and 1:2 stoichiometric ratios. Thus, the stoichiometric ratio of the ICs might be varied concerning the concentration. Both the guest molecules form ICs with a 1:1 ratio at lower concentrations (up to 8.0×10^{-3} M of β-CD) and a 1:2 ratio has been found at higher concentrations of β-CD. The binding constant for the formation of DABD:β-CD-ICs and BPT:β-CD-ICs in absorption spectra has been determined by analyzing changes in absorbance at a wavelength and fluorescence intensity with the influence of β-CD in terms of concentration.

The equilibrium of an IC formed for biphenyl compounds (BPT and DABD) with β-CD can be written as:

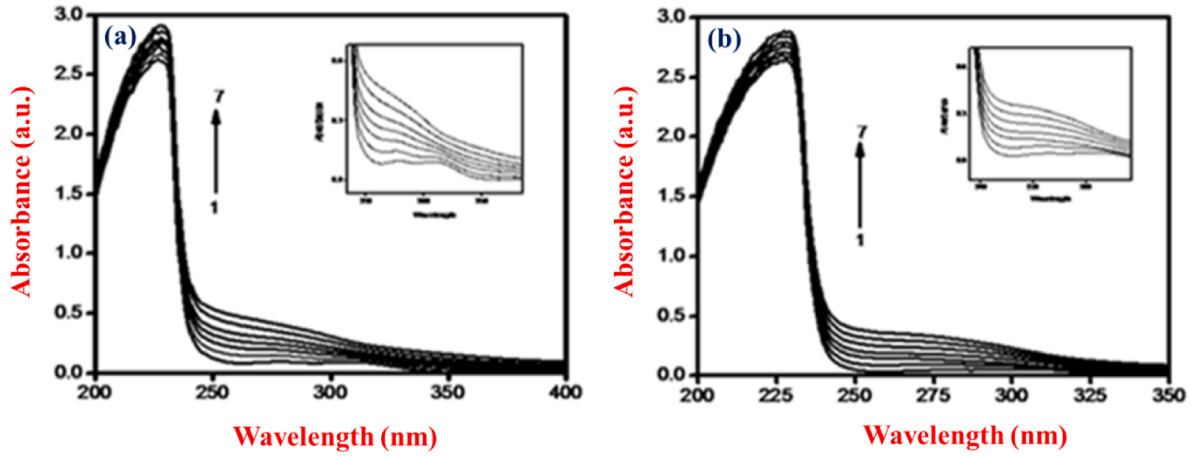

Fig. 1. UV spectra of BPT **(a)** and DABD, **(b)** (4.0×10^{-4} M) at different concentrations of β-CD in M. (1) Without β-CD, (2) 2.0×10^{-3}, (3) 4.0×10^{-3}, (4) 6.0×10^{-3}, (5) 8.0×10^{-3}, (6) 10.0×10^{-3} and (7) 12.0×10^{-3}.

Table 1
Absorption and fluorescence spectral data of BPT and DABD at different concentrations of β-CD in pH~**7**.

S. No.	Conc. of β-CD (M)	BPT			DABD		
		UV		Flu	UV		Flu
		λ_{max} (nm)	log ε	λ_{max} (nm)	λ_{max} (nm)	log ε	λ_{max} (nm)
1	Without	315	3.34		278	3.11	
		278	3.62	400			394
		229	4.81		229	4.82	
2	2.0×10^{-3}	316	3.43	473	278	3.39	
		276	3.64	349	229	4.82	396
		229	4.82				
3	4.0×10^{-3}	308	3.56	475	278	3.53	
		276	3.69	350	229	4.83	398
		230	4.83				
4	6.0×10^{-3}	302	3.65	476	279	3.65	
		275	3.71	351	230	4.83	398
		230	4.84				
5	8.0×10^{-3}	302	3.72	477	279	3.75	
		274	3.82	355	230	4.84	363
		230	4.84				
6	10.0×10^{-3}	302	3.80	477	279	3.83	
		273	4.12	354	230	4.84	351
		230	4.85				
7	12.0×10^{-3}	302	3.87	478	279	3.90	
		272	4.32	354	229	4.86	349
		228	4.86				
K : 1:1 (M^{-1})		40.1		93.52	54.4		704
K : 1:2 (M^{-1})		24,061		56,110	37,537		50,324
ΔG for 1:1 complex (kJ. mol^{-1})		−9.3		−11.43	−10.07		−16.52
ΔG for 1:2 complex (kJ. mol^{-1})		−25.42		−27.55	−26.5		−33.08

*Conc. : Concentration, Flu: Fluorescence.

$$\mathrm{DABD} + \beta - \mathrm{CD} \underset{(1:1\,\mathrm{ratio})}{\rightleftharpoons} \mathrm{DABD} : \beta - \mathrm{CD} - \mathrm{ICs} \underset{(1:2\,\mathrm{ratio})}{\rightleftharpoons} \mathrm{DABD} : 2\beta - \mathrm{CD} - \mathrm{ICs} \ldots\ldots \quad (5)$$

$$\mathrm{BPT} + \beta - \mathrm{CD} \underset{(1:1\,\mathrm{ratio})}{\rightleftharpoons} \mathrm{BPT} : \beta - \mathrm{CD} - \mathrm{ICs} \underset{(1:2\,\mathrm{ratio})}{\rightleftharpoons} \mathrm{BPT} : 2\beta - \mathrm{CD} - \mathrm{ICs} \ldots\ldots \quad (6)$$

The BH equation [46] can be used to calculate the binding constant 'K' and the stoichiometric ratios of the ICs of BPT and DABDwith β-CD. Figs. 2 and 3 depict a plot of $1/(A\text{-}A_0)$ as a function of 1/[β-CD] and $1/[\beta\text{-CD}]^2$ for the complexes with 1:1 and 1:2 ratios, respectively. The formation of 1:1 and 1:2 ICs is confirmed by a good linear correlation. The binding constant for the formation of ICs has been determined in both cases by analyzing changes in absorbance with respect to β-CD concentrations. K is calculated at room temperature (303.0 K) from the slope of BH plots and the values are provided in Table1.

The free energy change (ΔG) for the ICs can be calculated using the following equation from the values of 'K' (7),

$$\Delta G = -\mathrm{RT}\ln K \ldots\ldots \quad (7)$$

According to the ICs for the thermodynamic parameter, ΔG is negative, indicating that the inclusion process occurred spontaneously at 303.0 K, and the values are provided in Table 1.

The fluorescence intensities of BPT and DABD at pH 7.0 with various concentrations of β-CD are shown in Fig.4. The intensities in the fluorescence spectra of BPT are increased at the spectral maximum of 475.0 nm with respect to the concentration of β-CD. It suggested the formation of ICs [47–49]. The complexation is completed at a concentration of 12×10^{-3} M, and the fluorescence intensity does not change further. The BH [50] plot can be used to analyze the β-CD dependence spectra of BPT and DABD.

The linear plot is obtained by plotting $1/(I\text{-}I_0)$ *Vs* $1/[\beta\text{-CD}]$ for ICs with a 1:1 stoichiometric ratio and $1/(I\text{-}I_0)$) *Vs* $1/[\beta\text{-CD}]^2$ for ICs with a 1:2 ratio. The "K" value is calculated using the slope at the BH plots and Eq. (4). The BH plot (Fig. 5A) supports a good linear regression (r~0.989) for the ICs with a ratio of 1:1 (BPT:β-CD-ICs) and r ~0.988 for the ICs with a ratio of 1:2 (BPT:2β-CD-ICs). The fluorescence intensity decreased at a concentration of 8.0×10^{-3} M of β-CD, revealing an unusual behavior in the fluorescence spectra at 350.0 nm. This is due to the strain caused by the guest molecule's bending in the exited state, which causes the guest moiety to be expelled from the host molecule. This behavior does not result in complete exclusion due to the formation of a hydrogen bond between the substituent present in the third position of the guest molecule and the secondary alcohol present in the ribs of the host molecule. Because the 1:1 ICs predominate over the 1:2 complex at lower concentrations of β-CD, this effect is not observed.

The addition of β-CD increased the intensity of the DABD at the emission wavelength 400.0 nm, implying the formation of ICs with β-CD [51–53]. The complexation is complete at a concentration of 12.0×10^{-3} M, and no further changes in intensity occur. The BH [54] plot of 1:1 and 1:2 complexes are used to examine the β-CD influenced fluorescence intensities of the DABD. The BH plot (Fig. 5B) demonstrates a good linear regression (r ~0.986) for the 1:1 (DABD:β-CD-ICs) and (r~0.999) for the 1:2 (DABD:2β-CD-ICs) at ~400.0 nm.

A similar trend is observed for the ICs of DABD with β-CD according to the BPT:β-CD-ICs. The intensities at the concentration of β-CD (8.0 ×

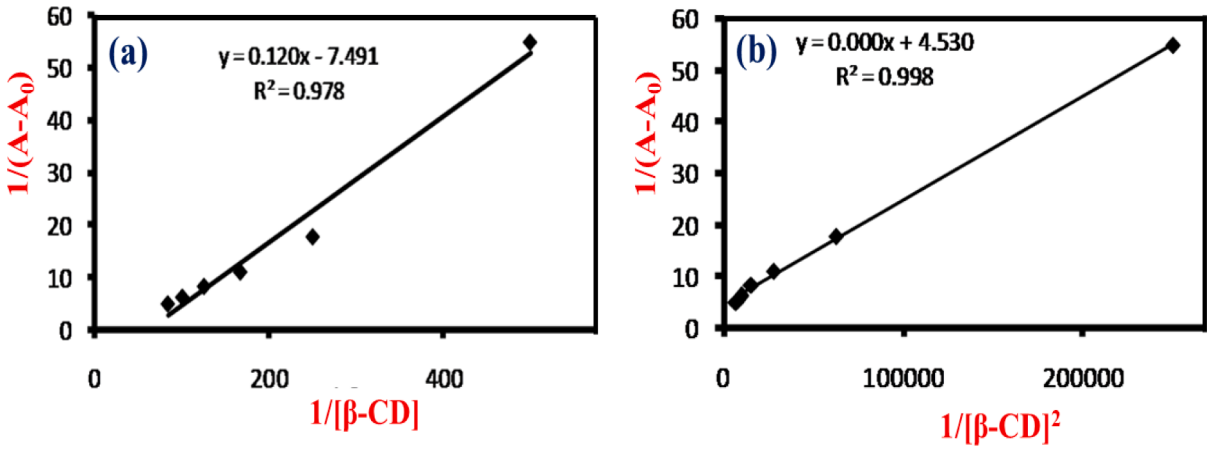

Fig. 2. BH absorption plot of BPT **(a)** $1/(A\text{-}A_0)$ *Vs* $1/[\beta\text{-CD}]$, and **(b)** $1/(A\text{-}A_0)$ *Vs* $1/[\beta\text{-CD}]^2$.

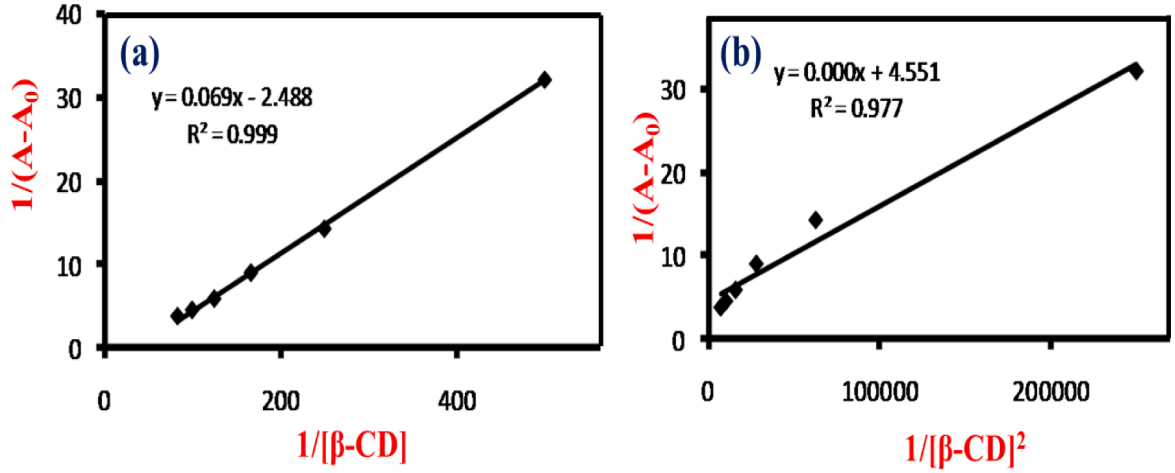

Fig. 3. BH absorption plot of DABD **(a)** $1/(A\text{-}A_0)$ *Vs* $1/[\beta\text{-CD}]$, **(b)** $1/(A\text{-}A_0)$ *Vs* $1/[\beta\text{-CD}]^2$.

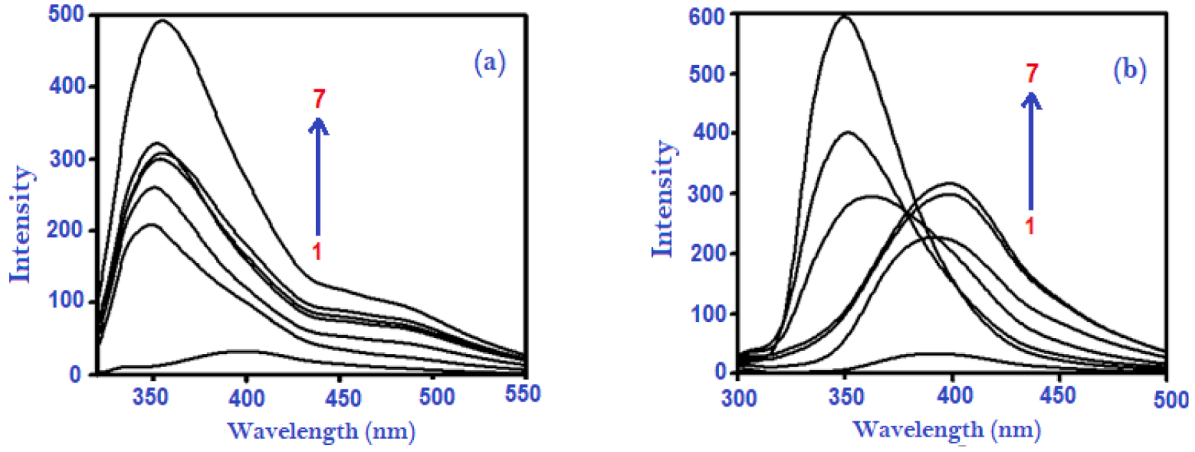

Fig. 4. Fluorescence spectra of BPT **(a)**, and DABD **(b)** (4.0×10^{-4} M) in different concentrations of β-CD in M (1) Without β-CD, (2) 2.0×10^{-3}, (3) 4.0×10^{-3}, (4) 6.0×10^{-3}, (5)8.0×10^{-3}, (6) 10.0×10^{-3} and (7) 12.0×10^{-3}.

10^{-3} M) show an unusual trend, with the peak position shifting from 400.0 to 350.0 nm. It provides the best linear regression plot for the formation of ICs with 1:1 and 1:2 ratios at both wavelengths. As a result, the shifts are caused by the expelling process within the aqueous medium, and the guest moiety is released from the host molecule due to strain caused by the guest molecule bending at the exited state. Because of the hydrogen bonding between the substituent in the third position of the guest molecule (DABD) and the secondary alcohol in the ribs of the host molecule (β-CD), this behavior does not result in complete exclusion. This effect is not observed at lower concentrations of β-CD; at these concentrations, 1:1 predominates over 1:2. Instead, the peak shift reveals differences in fluorescence intensity, indicating the presence of

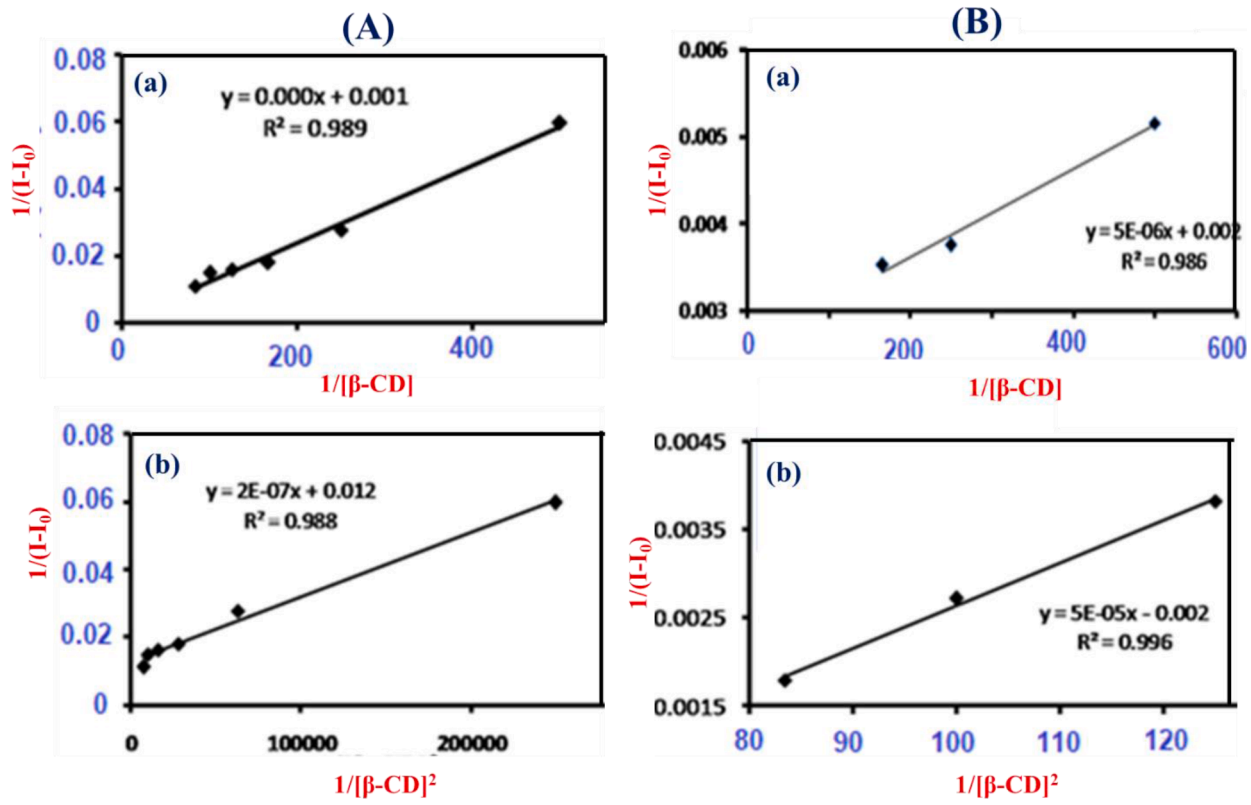

Fig. 5. BH plot of BPT **(A),** and DABD **(B)** : (a) $1/(I\text{-}I_0)$*Vs*$1/[\beta\text{-CD}]$, (b) $1/(I\text{-}I_0)$*Vs*$1/[\beta\text{-CD}]^2$.

intra and intermolecular hydrogen bonding in the DABD and the β-CD.

3.2. *Electrochemical studies*

Electrochemical analysis confirms the formation of ICs of BPT and DABD with β-CD, and a different electrochemical property is observed for the guest molecules with the β-CD involved [55,56]. The interaction of the β-CD with BPT as determined by (CV) analysis is depicted in Fig. 6 (a), and the relevant data is provided in Table 2. The electrochemical properties would have been different if β-CD had interacted with the guest molecule BPT. First, the BPT is placed in a solution of β-CD at pH 7.0 with adequate stirring. The CV is then completed. The CV graph is shown for the BPT as well as various concentrations of β-CD. The concentration of the BPT is kept constant at 2.0×10^{-2} M. The oxidation and reduction potentials of BPT are obtained in the absence of β-CD, with a peak potential, Ep_a at 0.226 V and Ep_c at 0.075 V *Vs* SCE at pH 7. The addition of β-CD shifts the electrode potential towards the higher potential, confirming the formation of ICs. Peak current decreased with increasing β-CD concentrations, which could be due to the formation of ICs. Similarly, the CV analysis of DABD with β-CD is made and shown in Fig. 6b, and the corresponding data is summarized in Table 2. In the absence of -CD, both DABD potentials are observed, with Ep_a at 0.334 V

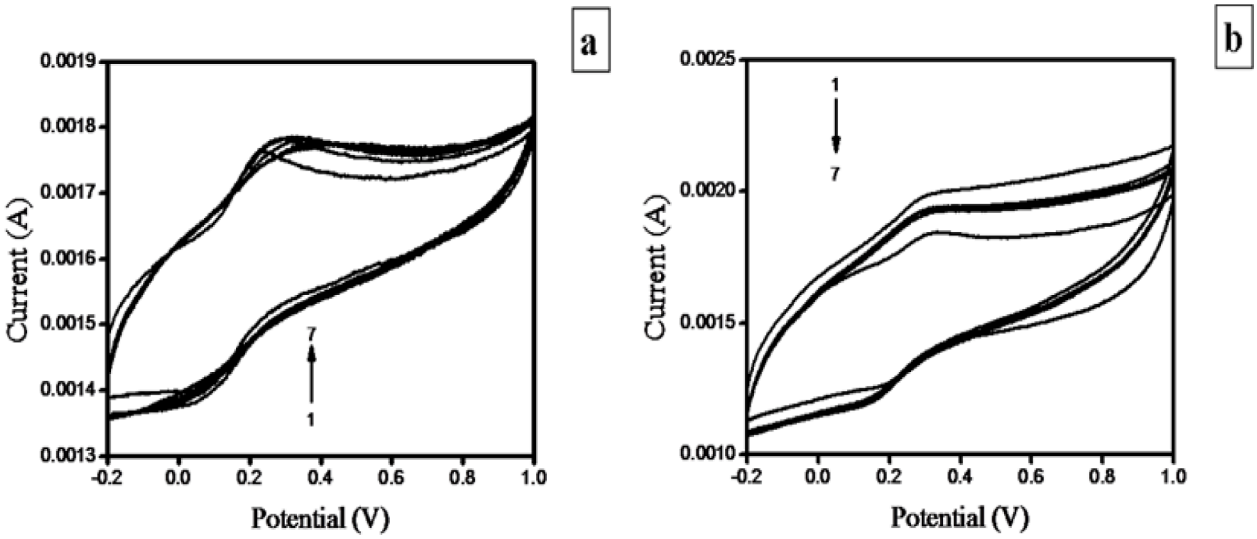

Fig. 6. Cyclic Voltammetry (CV) for BPT **(a)**, and DABD **(b)** (Conc. 2.0×10^{-4} M) at various concentrations of β-CD in M. (1) Without β-CD, (2) 2.0×10^{-3}, (3) 4.0×10^{-3}, (4) 6.0×10^{-3}, (5) 8.0×10^{-3}, (6) 10.0×10^{-3}, and (7) 12.0×10^{-3}.

Table 2
CV for BPT and DABD in pH~7 buffer, Scan rate 50 VS^{-1}, BPT and DABD (Concentration 2.0 × 10^{-}4 $mol.dm^{-3}$) solution at different concentrations of β-CD (0.0 – 12.0 × 10^{-3} M).

S. No.	Conc. of β-CD (M)	BPT				DABD			
		Ep_a (V)	Ip_a (μA)	Ep_c (V)	Ip_c (μA)	Ep_a (V)	Ip_a (μA)	Ep_c (V)	Ip_c (μA)
1	Without β-CD	0.226	93.02	0.0750	−74.4	0.334	84.02	0.194	−50.02
2	2.0 × 10^{-3}	0.265	86.83	0.0598	−66.71	0.294	47.49	0.153	−52.16
3	4.0 × 10^{-3}	0.283	71.32	0.0597	−66.7	0.309	25.24	0.152	−58.59
4	6.0 × 10^{-3}	0.311	68.21	0.0538	−63.63	0.312	23.89	0.149	−63.22
5	8.0 × 10^{-3}	0.331	59.03	0.0478	−54.25	0.316	14.95	0.148	−67.84
6	10.0 × 10^{-3}	0.341	54.25	0.0418	−38.72	0.319	14.65	0.146	−72.15
7	12.0 × 10^{-3}	0.377	38.73	0.0388	−37.19	0.323	14.42	0.134	−81.67

and Ep_c at 0.194 V *Vs* SCE at pH 7. The addition of β-CD shifts the electrode potential towards the higher potential, revealing the formation of ICs.

BH relationships are used to calculate the stoichiometric ratios (1:1 and 1:2) and "K" for the two ICs & 10).

$$\frac{1}{(I_{HG}-I_G)} = \frac{1}{\Delta I} + \frac{1}{K\ \Delta I[\beta - CD]} \quad \ldots\ldots \tag{9}$$

$$\frac{1}{(I_{HG}-I_G)} = \frac{1}{\Delta I} + \frac{1}{K\Delta I\ [\beta - CD]^2} \ldots\ldots \tag{10}$$

Here, I_G is the oxidation peak current of the BPT and DABD, I_{HG} is the oxidation peak current of (DABD:β-CD-ICs & BPT:β-CD-ICs), and (I_G-I_{HG}) is the difference between the oxidation peak current of the BPT, DABD, and respective ICs with β-CD. I is the difference between the molar peak current co-efficient of the guests, BPT and DABD, and ICs, $[DABD]_0$& $[BPT]_0$, and $[\beta\text{-CD}]_0$, respectively, are the initial concentrations of BPT, DABD, and β-CD. A straight line plot of $1/(I_G\text{-}I_{HG})$ *Vs* $1/[\beta\text{-CD}]$ and $1/(I_G\text{-}I_{HG})$ *Vs* $1/[\beta\text{-CD}]^2$ is shown in Fig. 7. The formation of ICs with 1:1 and 1:2 ratios is confirmed by good linear correlations.

K is calculated from the slopes for DABD:β-CD-ICs is 61.42 M^{-1} and BPT:β-CD-ICs is 478.93 M^{-1} for 1:1. Likewise, the binding constants for DABD:β-CD-ICs and BPT:β-CD-ICs are 30,708 and 28,735 M^{-1}, respectively. Beyond the maximum β-CD concentrations (12.0 × 10^{-3} M), the oxidation peak current remains constant. These findings indicated that the BPT molecule is included in the cavity of the β-CD and formed an ICs. The free energy change is calculated using the 'K' values as well. As can be seen, the G value for the ICs with a 1:1 ratio of DABD:β-CD and BPT:β-CD are found to be −10.37 and −15.55 $kJ.mol^{-1}$, respectively at pH7.0, whereas the G value for the ICs with 1:2 ratio of DABD:β-CD and BPT:β-CD is found to be −26.03 and −25.87 $kJ.mol^{-1}$, respectively at pH7.0, indicating that the ICs.

Taking into account all of the above interpretations, a possible mechanism for both ICs is now proposed. Naturally, the inclusion of the biphenyl ring into the cavity of β-CD allows the formation of ICs of biphenyl compounds with β-CD, and the functional group of guests

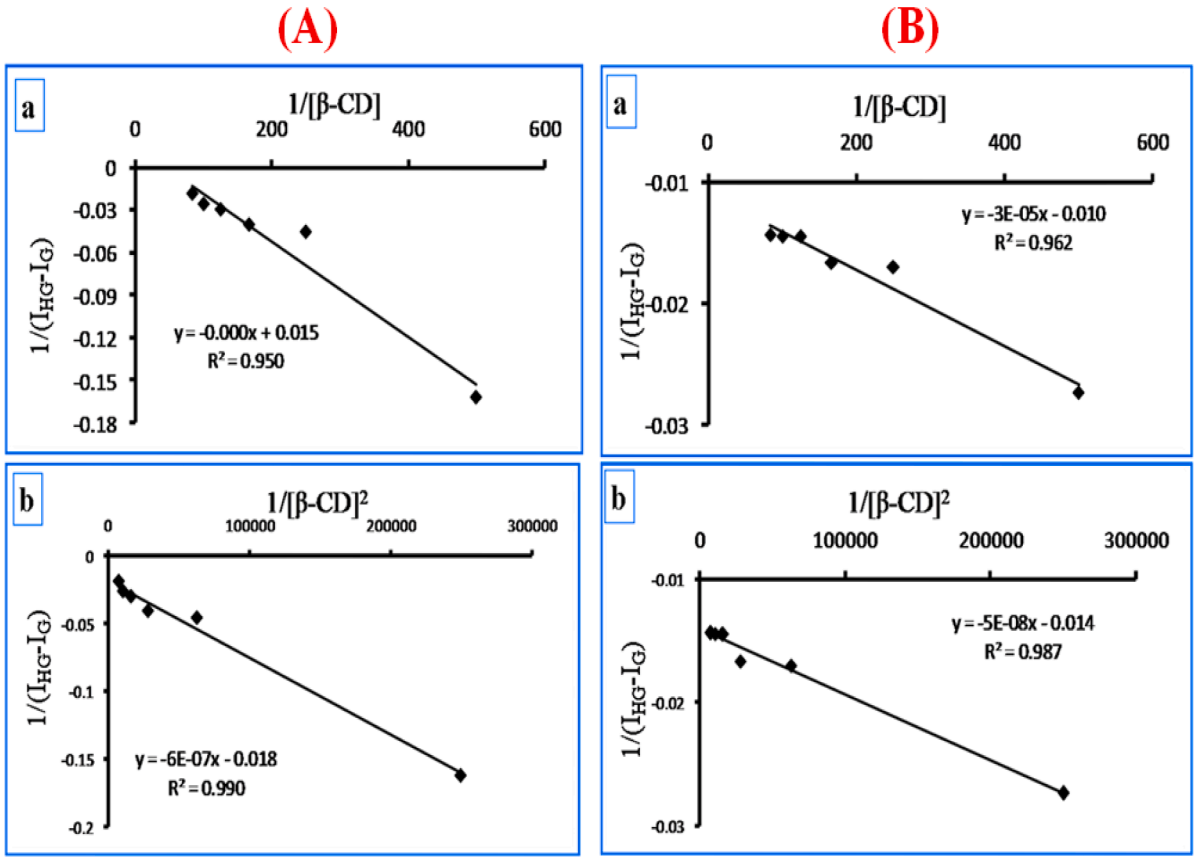

Fig. 7. BH voltammetric plots of BPT **(A),** and DABD **(B): (a)** $1/(I_{HG}\text{-}I_G)$ *Vs* $1/[\beta\text{-CD}]$, and **(b)** $1/(I_{HG}\text{-}I_G)$*Vs* $1/[\beta\text{-CD}]^2$.

interacts with the rim part of β-CD at pH 7.0. Scheme 1 clearly shows the formation of ICs with ratios of 1:1 and 1:2. One phenyl moiety of BPT is encapsulated into the cavity of β-CD in the 1:1 ICs, and the two amine groups in a phenyl ring are fully entrapped inside the β-CD. Hopefully, another phenyl ring with two amine groups is completely entrapped in the cavity of β-CD by ICs with a 1:2 ratio. The structure of ICs is further stabilized by the continuous release of water molecules from the hydrophobic cavity of the β-CD. The binding constant values show that the ICs are better in the exited state than in the ground state, which could be due to the favorable environment created by the molecule flipping inside the cavity of β-CD.

The ICs of DABD are encapsulated in the cavity of the β-CD cavity in a 1:1 ratio, and the amine and hydroxyl groups of the guest molecule are enclosed in the cavity of the β-CD. The IC structure gains additional stabilization energy by releasing water from the hydrophobic cavity, and the equilibrium can be notable for water replacement. The ICs of DABD have a 1:2 ratio, both phenyl rings are possibly encapsulated, and two numbers of β-CD are required. The binding constant also clearly revealed the superior inclusion in the exited state over the ground state, which could be attributed to the deeper inclusion of the guest molecule, DABD, into the cavity of the host, β-CD. Finally, when the ICs are made with 1:2, both have better binding constants and are more stable and favorable.

3.3. Characterizations of ICs in solid state

Powder XRD analysis is used to inspect the formation of ICs and is a convenient method for confirming ICs. The nature of substances is changing as a result of this formation. For example, the complete disappearance or shift to some diffraction angles can transform crystalline to amorphous and vice-versa [57,58].

The powder XRD patterns of BPT, β-CD, and ICs prepared by the co-precipitation method with a 1:2 ratio are shown in Fig. 8a. The XRD patterns for the BPT revealed several sharp, high-intensity peaks at different diffraction angles (2θ) of 17.1, 18.4, 27.6, 42.8, and 47.3, indicating their nature as crystalline. The crystalline diffractogram and ICs revealed a diffuse halo pattern, indicating that the product is amorphous in nature, according to the β-CD. The ICs' diffraction patterns correspond to the exact position of pure BPT as well as the β-CD. The low intensities in the respective diffraction peaks indicated that the particle sizes had been reduced following the ICs.The XRD patterns of DABD and ICs are shown in Fig. 8b. The presence of several sharp peaks with high intensity at different diffraction angles (2θ)of 15.5, 17.1, 20.7, 28.2, 29.2, and 31.3 in DABD. XRD patterns suggested that DABD existed as crystalline in nature. Individual molecules in ICs have lost their crystallinity due to their amorphous nature. The lower diffraction peak intensities indicate that particle sizes are reduced during the formation of ICs. The typical diffraction pattern indicates that DABD in ICs is completely amorphous. The ICs and crystalline nature of BPT and DABD have vanished after they have undergone amorphization. The typical diffuse pattern clearly demonstrates the formation of ICs.

SEM measurement is well suited for surface visualization, particularly when surface feature sizes are far below three microns [58]. SEM analysis is used to measure surface roughness and visualize surface area at the nanoscale. The clear stone-like surface morphological structure of β-CD is observed (Fig. 9a). Similarly, SEM images of BPT, DABD, and respective ICs are shown in Fig. 9b-9e. Images clearly show the distinction between the ICs and raw materials of guests, BPT and DABD, and host β-CD. The images show that the surface of the guest molecules has been significantly modified after forming ICs [59,60]. As a result, these modifications can be taken as proof of the formation of ICs.

The thermal analysis includes DTA and it provides further supportive pieces of evidence for the ICs. When guest molecules are encapsulated into the cavity of β-CD or in the crystal lattice, their melting, boiling, or sublimation points are generally shifted or disappeared within the temperature range where β-CD decomposes [45,46]. The DTA of BPT revealed a sharp endothermic peak at 179.95 °C (Fig. 10a), representing the melting point of BPT, and a sublimation peak at 371.63 °C. In the case of β-CD (Fig. 10a), a broad endothermic peak at around 90.86 °C is observed, which may be the cause of the dehydration process. There is also a continuous broad endothermic peak at 336.00 °C, which is attributed to β-CD decomposition. There are three peaks visible in the DTA of the ICs. The first peak appears at 98.48 °C and represents the dehydration of water molecule from the sample ICs, the second one is an endothermic peak for the BPT at 174.08 °C, and the third peak appears at 352.20 °C and represents the β-CD. The changes in temperature indicates the formation of the ICs [61].

The DTA curves revealed a sharp endothermic peak at 302.17 °C (Fig. 10b), indicating the decomposition of DABD. There are three peaks noticeable in the DTA of the ICs. The first one is at 89.21 °C, representingthe dehydration of water molecule; the second one is at 287.96 °C, representing the presence of DABD; and the third is at

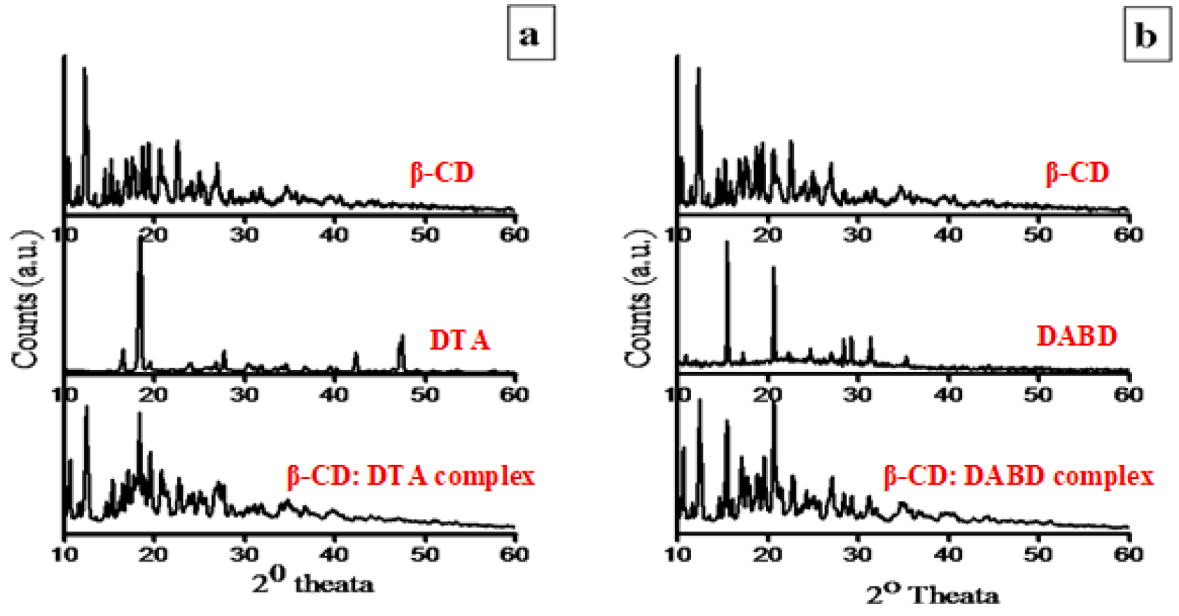

Fig. 8. Powder XRD of **(a)** β-CD, BPT and its ICs, **(b)** β-CD, DABD and its ICs.

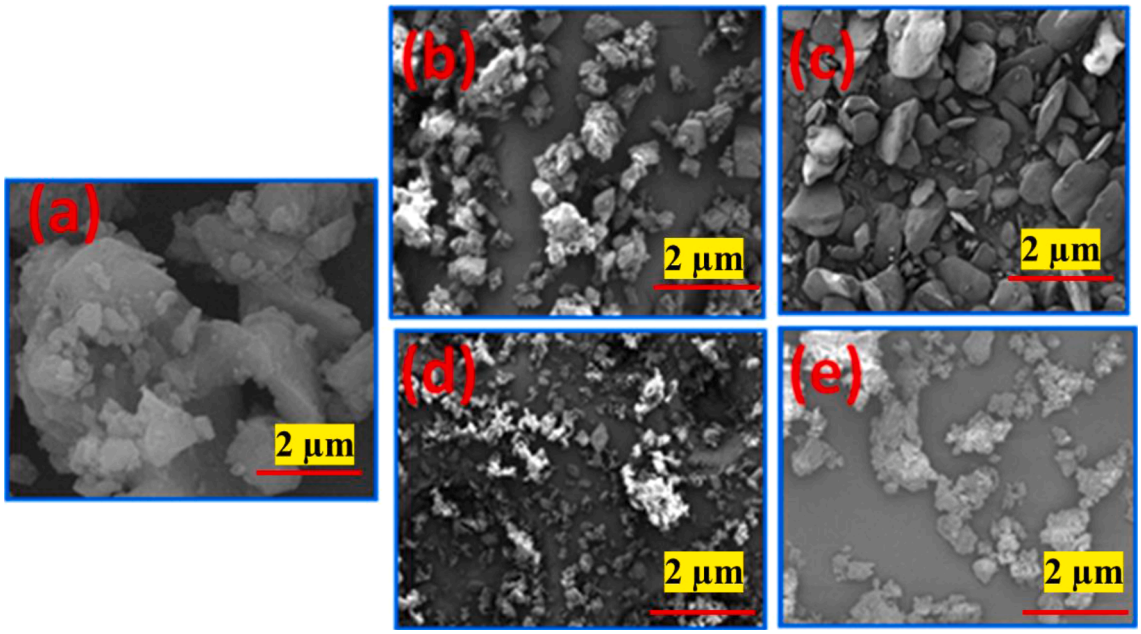

Fig. 9. SEM photographs (Pt. coated) of **(a)** β-CD, **(b)** BPT, **(c)** ICs of BPT, **(d)** DABD, and **(e)** ICs of DABD.

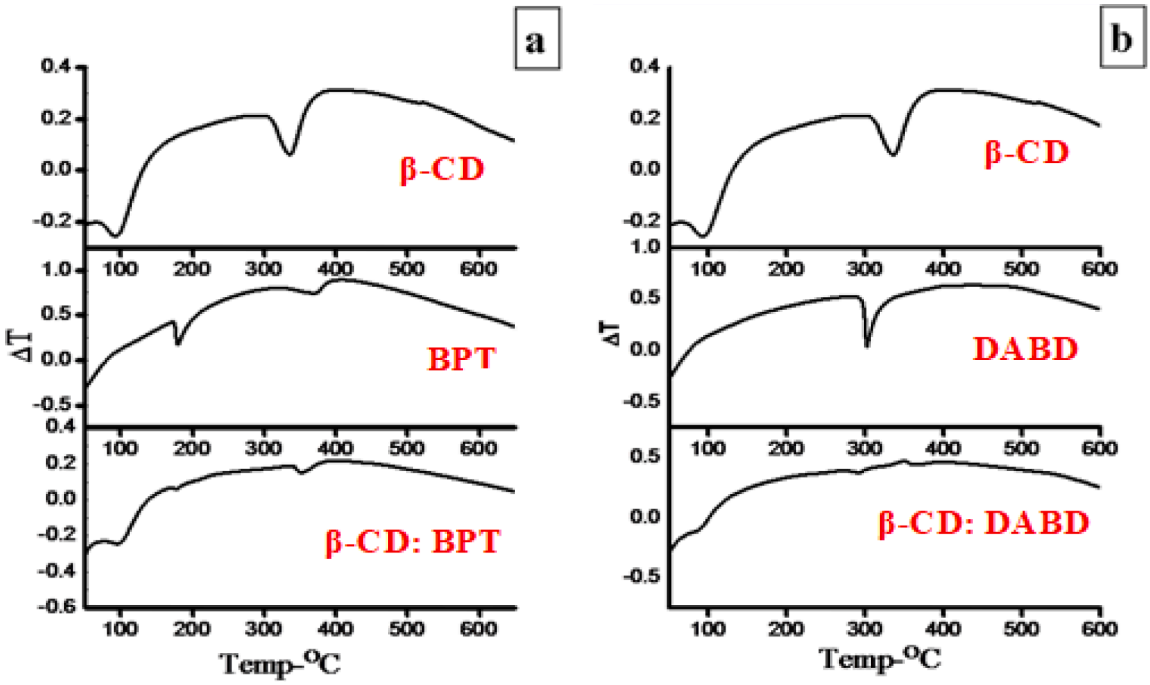

Fig. 10. DTA curves of **(a)** β-CD, BPT, and ICs, **(b)** β-CD, DABD and ICs.

327.02 °C, representing the presence of β-CD. The decomposition of the ICs is revealed by a peak at 366.08 °C. The changes in temperature could be physical evidence for the ICs [61].

FT-IR spectral interpretation is mainly used to characterize ICs in terms of functional groups and also group frequencies. During the analysis, some of the bands are generally shifted or else some of the intensities changed to some extent, resulting in the formation of ICs and providing information about the inclusion of the guest molecule into the cavity of the host [48,49]. The selective stretching groups of BPT are aromatic NH stretching, aromatic NH bending vibration, aromatic C—H stretching, and aromatic C═C stretching appear at 3354, 1496, 2990, and 2870 cm^{-1}, respectively (Fig. 11a). Furthermore, C—C stretching at the phenyl group junction appears at 1628 cm^{-1}, and C—C bending vibration appears at 1161 cm^{-1}. The stretching frequencies mentioned above are shifted to 3357 and 1499 cm^{-1} in the ICs. Peaks at 2879, 1634, and 1156 cm^{-1} have vanished. The shift in wave number and disappearance of the C—H stretching revealed that the BPT is entrapped in the cavity of β-CD. The C—O-C bending at 1029 cm^{-1} is not disturbed in the ICs, indicating that the BPT is included in the axial within the cavity of β-CD.

The aromatic C—H stretching is observed at 3001 cm^{-1}, the aromatic C═C stretching is observed at 2886 cm^{-1}, and the phenolic -OH stretching are observed at 3355 cm^{-1} for DABD. C—C stretching at the phenyl group junction at 1596 cm^{-1}, aromatic OH bending at 1508

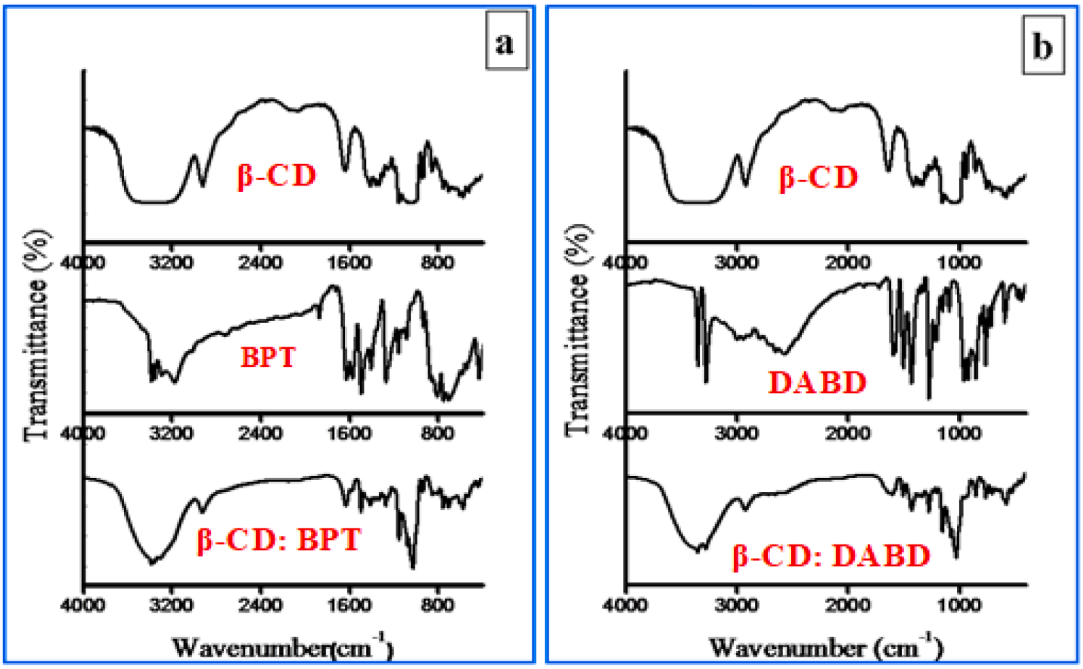

Fig. 11. FT-IR spectra of **(a)** β-CD, BPTand ICs, **(b)** β-CD, DABD, and ICs in KBr.

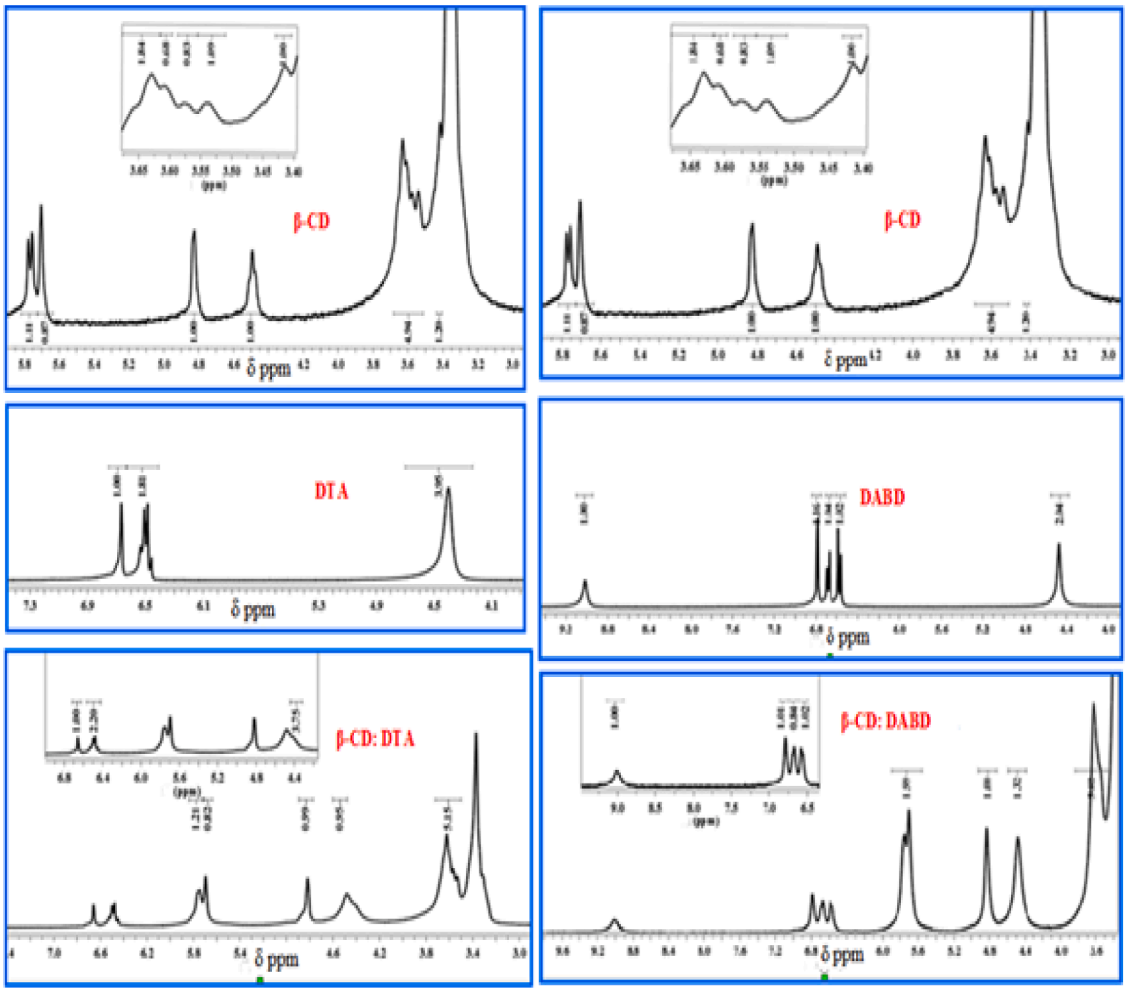

Fig. 12. [1]H NMR spectra of β-CD, BPT, DABD, and its ICs.

cm^{-1}, aromatic NH stretching at 3282 cm^{-1}, C—C bending vibration at 1155 cm^{-1}, and aromatic NH bending at 1508 cm^{-1} are obtained (Fig. 11b) and are shifted to broader, disappeared, 2926, 1606, 1509, 3284, 1156, and 1509 cm^{-1}, respectively. The change in wave number, decrease in intensity, and broadening of a few peaks indicate that the DABD is encapsulated in the cavity of β-CD. The C—O—C bending vibration appears at 1029 cm^{-1} and is not disturbed during complexation, representing the DABD is included with the axial position in the β-CD molecule.

The most powerful technique for studying the interaction between guest molecules and ICs is ^{1}H NMR spectroscopy, which is also used to confirm IC conformations. The ^{1}H NMR analysis reveals the chemical shifts of β-CD in the hydrogen atoms as well as the chemical shifts caused by ICs. In general, in the ICs, β-CD protons located within the cavity (H-3 and H-5) show remarkably large shifts. Although H-1, H-2, H-4, and H-6 on the outside of β-CD show a minor shift. The chemical shift data for the ICs differs from that of the free components of the guest and host.

The details of the chemical shift of the BPT, β-CD, and ICs are shown in Fig. 12 & Table 3. The chemical shift of BPT shows an up-field shift on complexation except $–NH_2$ showing the presence of the guest molecule inside the cavity of the β-CD. Considering the β-CD also shows an up-field shift during complexation. The shift of H-3 is not observed in the ICs but the shift of H-5 is remarkably high since they are present in the interior of the cavity. This is solid evidence for the inclusion of guest molecules in the cavity of the host. Similarly, the chemical shifts of the DABD, β-CD and ICs are shown in Fig. 12 & Table 3. The chemical shift of DABD shows an up-field shift during complexation which is evidence of the formation of ICs. When the β-CD is considered, it also exhibits an up-field shift during complexation. Because H-3 and H-5 are present in the host's interior cavity, their chemical shifts are remarkably high. This is strong evidence that the guest molecule is trapped in the host's cavity. The β-CD's up-field shift is caused by the host molecule's conformational rearrangement. The majority of the chemical shifts in the above-specified signal are shifted by about 1 ppm towards the shielding region.

3.4. Antibacterial assay

The antibacterial assay [50] is used to detect gram-positive and gram-negative bacteria pathogens. For the pathogenic study, *Escherichia coli* (*E. coli*) and *Staphylococcus aureus* (*S. aureus*) are used as gram-negative and gram-positive bacterial strains, respectively. For the stock solution, the solid ICs are dissolved in DMSO at a concentration of 2.0 mg per 50 ml.

A few sterile petri dishes are filled with nutrient agar medium and allowed to solidify. Swipe the *E. coli* and *S. aureus* microbes in the Petri dishes and incubated for five hours. Bacterial lawns cover the surface of the nutrient agar plates. Five wells are made that are equidistant from each other using a sterile gel puncher. Three identical concentrations and volumes of ICs, analytes, and β-CD are added to the well and placed in an incubator at 37 °C for 24 h. The zone inhibition around the well is measured after 24 h. All of this is done in an aseptic environment.

The observations using BPT and ICs against gram-positive are shown in Fig.13. From the figure, the ICs prepared by the solution method show significant antibacterial activity against the gram-positive bacteria, and the other ICs showed very low activity or no activity on the pathogen. Whereas in gram-negative bacteria (Fig. 13), the ICs prepared by solution and PM show more predominant activity than the KM products. The observations using DABDand ICs against gram-positive are shown in Fig. 13. From the figure, clearly shows the ICs by solution method show more significant anti-bacterial activity against the gram-positive bacteria than the other products like PM and KM. Fig. 13 depicts the results of the antibacterial assay using BPT and its respective ICs against gram-positive and gram-negative bacteria. According to the figure, the SE product has significant activity against gram-positive bacteria, whereas the other ICs have very low or no activity. In gram-negative bacteria, SE product and PM exhibited greater activity than KM product.

4. Conclusions

We successfully obtained the ICs of BPT and DABD with β-CD in the aqueous and solid phases in this current research approach. The obtained results are clearly explained using UV and fluorescence analysis, and their respective changes by the addition of CD have been used to calculate the binding constant and stoichiometric ratio. FT-IR, XRD, SEM, DSC, and ^{1}H NMR spectral techniques are used to characterize the ICs. Furthermore, both ICs have better antibacterial activity against gram-positive and gram-negative bacterial strains, implying that the prepared ICs would be a better material for food packaging and pharmaceutical applications.

5. Author statement

The contributions of all authors must be described in the following manner:

The authors confirm their contribution to the paper as follows:

Study conception, design & Interpretation of results: **Kumaraswamy Paramasivaganesh**

Draft manuscript review: **Vimalasruthi Narayanan**

Draft manuscript review: **Vigneshkumar Ganesan**

Draft manuscript review: **Esakkimuthu shanmugasundram**

Draft manuscript review & Editing: **Rajaram Rajamohan**

Review & Editing: **Yong Rok Lee**

Table 3
^{1}H NMR chemical shifts of the β-CD, BPT, and DABD protons in the presence and absence of β-CD.

β-CD Protons	BPT			DABD		
	BPT	ICs	Δδ	DADB	ICs	Δδ
H1	4.824	4.8197	−0.0043	4.824	4.8271	0.0031
H2	3.4149	–	–	3.4149	–	–
H3	3.6066	–	–	3.6066	3.6146	0.0080
H4	3.5375	3.5329	−0.0046	3.5375	3.5443	0.0068
H5	3.5704	3.5613	−0.0091	3.5704	3.5817	0.0113
H6	3.6298	3.6219	−0.0079	3.6298	3.6280	−0.0018
OH2	5.7754	5.7621	−0.0133	5.7754	5.7526	−0.0228
OH3	5.7024	5.6968	−0.0056	5.7024	5.6973	−0.0051
OH6	4.4914	4.4853	−0.0061	4.4914	4.4792	−0.0122

Proton	BPT				DABD				
	$-NH_2$	H2	H5	H6	-OH	$-NH_2$	H2	H5	H6
Guest	4.3996	6.5075	6.4839	6.6678	9.0146	4.4700	6.7889	6.671	6.5863
ICs	4.4147	6.4989	6.4764	6.6583	9.0082	–	6.785	6.5863	6.5849
Δδ	0.0151	−0.0086	−0.0075	−0.0095	−0.0064	–	−0.0039	−0.0847	−0.0014

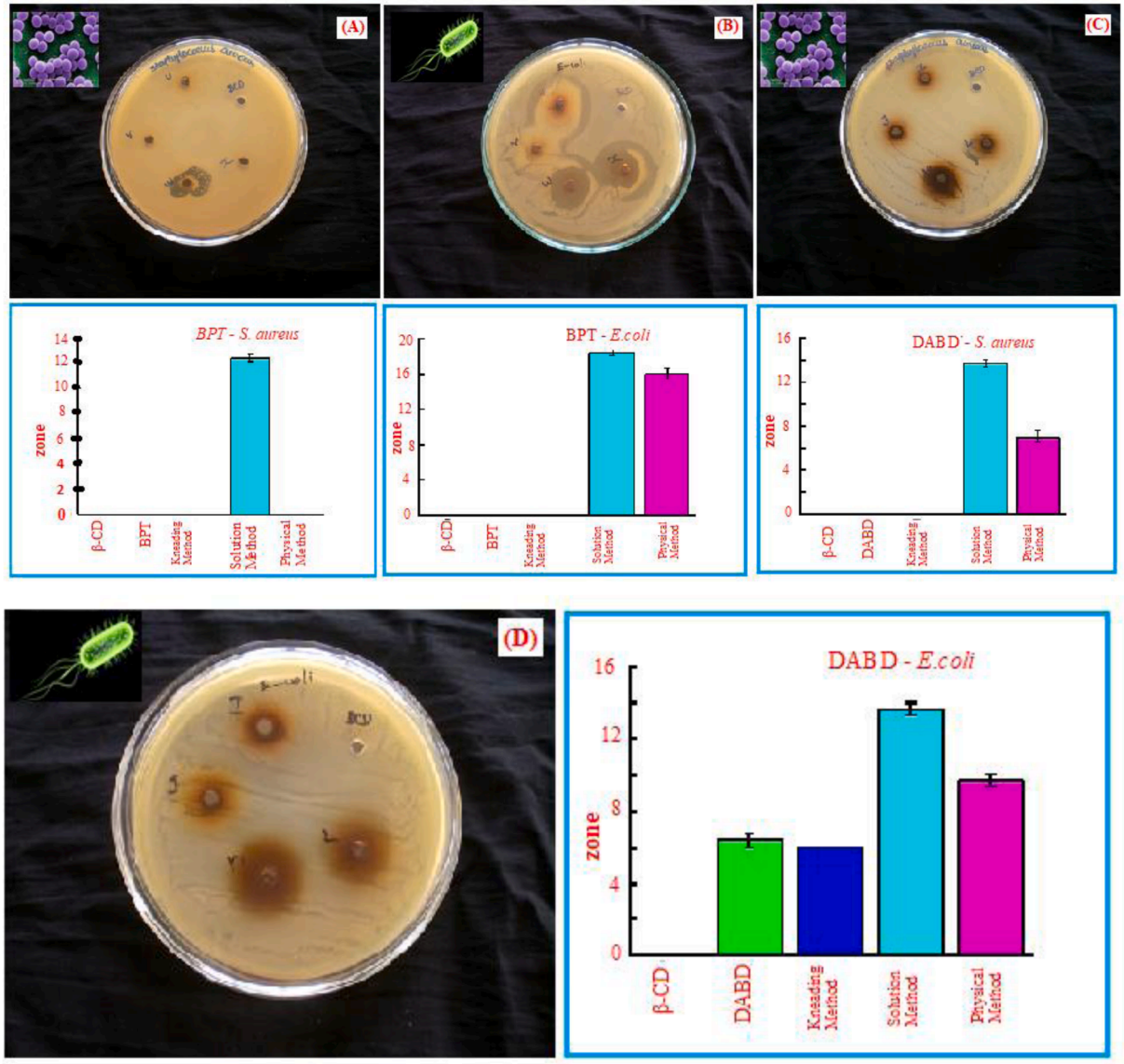

Fig. 13. Zone of inhibition and test photograph of antibacterial activity (*S. aureus* and *E. coli*) on β-CD, BPT, DABD, KM, ICs, and PM products.

Review, Editing & Supervisor: **Stalin Thambusamy**

All authors reviewed the results and approved the final version of the manuscript.

Declaration of Competing Interest

The authors declare that they have no known competing financial interests or personal relationships that could have appeared to influence the work reported in this paper. As the authors of this manuscript, we all have no conflict of interest in the present work. On behalf of all the authors for declared our interest and who are all involved in making this article, I have put my signature and forwarded this for consideration for publication in your esteemed journal.

Data availability

Data will be made available on request.

Acknowledgments

Dr. Stalin, thank you very much to the Science and Engineering Research Board (SERB), Government of India. The paperwork funded by SERB File No.: EEQ/2018/001455. And likes to RUSA Phase 2.0 grant No. F. 24-51/2014-U, Policy (TNMulti-Gen), Dept. of Edn., Govt. of India, Dt.09.10.2018, TNRUSA, Chennai, TAMILNADU, and ALU, Dt.16.12.2022.

References

[1] J. Lemire, J. Harrison, R. Turner, Antimicrobial activity of metals: mechanisms, molecular targets and applications, Nat. Rev. Microbiol. 11 (2013) 371–384.
[2] E. Tfouni, M. Krieger, B.R. McGarvey, D.W. Franco, Structure, chemical and photochemical reactivity and biological activity of some ruthenium amine nitrosyl complexes, Coord. Chem. Rev. 236 (2003) 57–69.
[3] L. Pourcel, J. Routaboul, V. Cheynier, L.L. Debeaujon, Flavonoid oxidation in plants: from biochemical properties to physiological functions, Trends Plant Sci. 12 (2007) 29–36.
[4] C. ereiraFde, C.A. Vilanova-Costa, A.P. de Lima, S. Ribeiro Ade, H.D. da Silva, L. A. Pavanin, P. SilveiraLacerda Ede, Cytotoxic and genotoxic effects of cis-tetraammine(oxalato)ruthenium(III) dithionateon the root meristem cells of Allium cepa, Biol. Trace Elem. Res. 128 (2009) 258–268.

[5] A.K. Perevoshchikova, I.A. Nichugovskiy, A.K. Isagulieva, N.G. Morozova, I. V. Ivanov, M.A. Maslov, A.A. Shtil, Synthesis of novel lipophilic tetraamines with cytotoxic activity, Mendeleev Comm. 29 (2019) 616–618.

[6] O.K. Onajole, Y. Coovadia, T. Govender, H.G. Kruger, G.E. Maguire, D. Naidu, N. Singh, P. Govender, In vitro antifungal and antibacterial activities of pentacycloundecane tetra-amines, Chem. Biol. Drug Des. 77 (2011) 295–299.

[7] X. Xin Zhang, S. Jerald, M.R. Bradshaw, Enantiomeric recognition of amine compounds by chiral macrocyclic receptors, Chem. Rev. 97 (1997) 3313–3362.

[8] M.R. Maurya, C. Haldar, S. Behl, N. Kamatham, F. Avecilla, Copper (II) complex of monobasic tridentate ONN donor ligand: synthesis, encapsulation in zeolite-Y, characterization, and catalytic activity, J. Coord. Chem. 17 (2011) 2995.

[9] M. Barnali, N. Kamatham, S.R. Samanta, P. Jagadesan, J. He, V. Ramamurthy, Synthesis, characterization, guest inclusion and photophysical studies of gold nanoparticles stabilized with acid groups of organic cavitands, Langmuir 41 (2013) 12703.

[10] N. Kamatham, D.C. Mendes, J.P. Da Silva, R.S. Givens, V. Ramamurthy, Photorelease of incarcerated caged acids from hydrophobic coumaryl esters into aqueous solution, Org. Lett. 21 (2016) 5939.

[11] N. Kamatham, J.P. Da Silva, R.S. Givens, V. Ramamurthy, Melding caged compounds with supramolecular containers: the photogeneration and miscreant behavior of coumarylmethyl carbocation, Org. Lett. 13 (2017) 3588.

[12] A. Das, G. Sharma, N. Kamatham, R. Prabhakar, P. Sen, V. Ramamurthy, Ultrafast solvation dynamics reveal the octa acid capsule's interior dryness, J. Phys. Chem. A 123 (2019) 5928–5936.

[13] A. Shanmuga Priya, J. Sivakamavalli, B. Vaseeharan, R. Rajamohan, Y.R. Lee, S. Thambusamy, Interaction of torsemide with native cyclodextrin through inclusion complexation: In-vitro drug release, antibacterial and antibiofilm activities, J. Mol. Struc. 1286 (2023) 135624.

[14] C. Leelasabari, R. Rajamohan, Y.R. Lee, A. Subramania, K. Sivakumar, M. Murugan, G. Manigandan, Characterization and Molecular Docking Analysis for the Supramolecular Interaction of Lidocaine with β-Cyclodextrin, Polycyc. Arom. Comp. 43 (2023) 1202–1218.

[15] N.A. Tcyrulnikov, R. Varadharajan, A.A. Tikhomirova, M. Pattabiraman, V. Ramamurthy, R. Marshall Wilson, Modulation of reduction potentials of bis (pyridinium)alkanedications through encapsulation within cucurbit [7]uril, J. Org. Chem. 84 (2019) 8759–8765.

[16] B. Christin Maria, A. Ashwin, A. Vinothini, T. Stalin, P. MuthuMareeswaran, Synthesis of a safranin T-*p*-Sulfonatocalix[4]arene complex by means of supramolecular complexation, ChemistrySelect 2 (2017) 931–936.

[17] T. Chatterjee, M. Sarma, S.K. Das, Supramolecular architectures from ammonium-crown ether inclusion complexes in polyoxometalate association: synthesis, structure, and spectroscopy, Cryst. Growth Des. 10 (2010) 3149–3163.

[18] J. Lang, J.J. Dechter, M. Effemey, J. Kowalewski, Dynamics of an inclusion complex of chloroform and cryptophane-E: evidence for a strongly anisotropic van der waals bond, J. Am. Chem. Soc. 123 (2001) 7852–7858.

[19] M. Banjare, K. Behera, R. Banjare, S. Pandey, K.K. Ghosh, Inclusion complexation of imidazolium-based ionic liquid and β-cyclodextrin: a detailed spectroscopic investigation, J. Mol. Liq. 302 (2020), 112530.

[20] S. Gao, Y. Liu, J. Jiang, Q. Ji, Y. Fu, L. Zhao, C. Li, F. Ye, Physicochemical properties and fungicidal activity of inclusion complexes of fungicide chlorothalonil with β-cyclodextrin and hydroxypropyl-β-cyclodextrin, J. Mol. Liq. 293 (2019), 111513.

[21] W. Kang, H. Zhang, Y. Lu, H. Yang, T. Zhu, X. Zhang, C. Chen, B. Sarsenbekuly, Z. Besembaevna, Study on the enhanced viscosity mechanism of the cyclodextrin polymer and betaine-type amphiphilic polymer inclusion complex, J. Mol. Liq. 296 (2019), 111792.

[22] B. Rajbanshi, A. Dutta, B. Mahato, D. Roy, D. Maiti, S. Bhattacharyya, M.N. Roy, Study to explore host guest inclusion complexes of vitamin B1 with CD molecules for enhancing stability and innovative application in biological system, J. Mol. Liq. 298 (2020), 111952.

[23] K. Kaur, R. Jindal, D. Jindal, Synthesis, characterization and studies on host-guest interactions of inclusion complexes of metformin hydrochloride with β–cyclodextrin, J. Mol. Liq. 282 (2019) 162–168.

[24] T.A. Andrade, T.S. Freitas, F.O. Araújo, P.P. Menezes, G. Anne, A. Dória, A. S. Rabelo, L.J. Quintans-júnior, M.R.V. Santos, D.P. Bezerra, Physico-chemical characterization and antibacterial activity of inclusion complexes of Hyptismartiusii Benth essential oil in β-cyclodextrin, Biomed. Pharmacother. 89 (2017) 201–207.

[25] Y. Guang-Fu, W. Hong-Bo, Y. Wen-Chao, G. Daquan, Zhan Chang-Guo, Bioactive permethrin/β-cyclodextrin inclusion complex, J. Phys. Chem. B 110 (2006) 7044–7048.

[26] M. Paczkowska, M. Mizera, K. Sałat, A. Furgała, P. Popik, J. Knapik-Kowalczuk, A. Krause, D. Szymanowska-Powałowska, Z. Fojud, M. Kozak, M. Paluch, J. Cielecka-Piontek, Enhanced pharmacological efficacy of sumatriptan due to modification of its physicochemical properties by inclusion in selected cyclodextrins, Sci. Rep. 8 (2018) 16184.

[27] E.V.R. Campos, P.L.F. Proença, J.L. Oliveira, C.C. Melville, J.F. Della Vechia, D. J. de Andrade, L.F. Fraceto, Chitosan nanoparticles functionalized with β-cyclodextrin: a promising carrier for botanical pesticides, Sci. Rep. 8 (2018) 2067.

[28] M.I. Sancho, M.G. Russo, M.S. Moreno, E. Gasull, S.E. Blanco, G.E. Narda, Physicochemical characterization of 2-hydroxybenzophenone with β-cyclodextrin in solution and solid state, J. Phys. Chem. B 119 (2015) 5918–5925.

[29] S. Ferro, G. Jori, S. Sortino, R. Stancanelli, P. Nikolov, G. Tognon, F. Ricchelli, A. Mazzaglia, Inclusion of 5-[4-(1-D*odecanoylpyridinium*)]-10,15,20-triphenylporphine in supramolecular aggregates ofcationic amphiphilic cyclodextrins: physicochemical characterization of the complexes and strengthening of the antimicrobial photosensitizing activity, Biomacromolecules 10 (2009) 2592–2600.

[30] X. Han, Z. Zhang, H. Shen, J. Zheng, G. Zhang, Comparison of structures, physicochemical properties and in vitro bioactivity between ferulic acid-β-cyclodextrin conjugate and the corresponding inclusion complex, Food. Res. Int. 125 (2019), 108619.

[31] K. Srinivasan, K. Kayalvizhi, K. Sivakumar, T. Stalin, Study of inclusion complex of β-cyclodextrin and diphenylamine; photophysical and electrochemical behaviours, Spectrochim. Acta A 79 (2011) 169–178.

[32] K. Srinivasan, J. Vaheethabanu, P. Manisankar, T. Stalin, Study of inclusion complex of β-cyclodextrin and ortho-anisidine; photophysical and electrochemical behaviours, J. Mol. Struct. 987 (2011) 214–224.

[33] K. Srinivasan, T. Stalin, K. Sivakumar, Spectral and electrochemical study of host–guest inclusion complex between 2,4-dinitrophenol and β-cyclodextrin, Spectrochim. Acta A 94 (2012) 89–100.

[34] K. Paramasivaganesh, K. Srinivasan, A. Manivel, S. Anandan, K. Sivakumar, S. Radhakrishnan, T. Stalin, Studies on inclusion complexation between 4,4-dihydroxybiphenyl and β-cyclodextrin by experimental and theoretical approach, J. Mol. Struct. 1048 (2013) 399–409.

[35] A. Shanmuga Priya, B. Suganya Bharathi, G. Vigneshkumar, M. Maniyazagan, K. Sakthivelu, N. Vimalasruthi, B. Vaseeharan, J. Sivakamavalli, S. Thambusamy, In-vitro dissolution and microbial inhibition studies on anticancer drug etoposide with β-cyclodextrin, Mat. Sci. Eng. C 102 (2019) 96–105.

[36] A. Shanmuga Priya, B. Suganya Bharathi, G. Veerakanellore, T. Stalin, In-vitro dissolution rate and molecular docking studies of cabergoline drug with β-cyclodextrin, J. Mol. Struct. 1160 (2018) 1–8.

[37] A. Shanmuga Priya, J. Sivakamavalli, B. Vaseeharan, T. Stalin, Improvement on dissolution rate of inclusion complex of Rifabutin drug with β-cyclodextrin, Int. J. Biol. Macromol. 62 (2013) 472–480.

[38] S. Gao, W. Feng, H. Sun, L. Zong, X. Li, L. Zhao, F. Ye, Y, Fabrication and characterization of antifungal hydroxypropyl-β-cyclodextrin/pyrimethanil inclusion compound nanofibers based on electrospinning, J. Agric. Food Chem. 70 (26) (2022) 7911–7920.

[39] Z.I. Yildiz, A. Celebioglu, M.E. Kilic, et al., Fast-dissolving carvacrol/cyclodextrin inclusion complex electrospun fibers with enhanced thermal stability, water solubility, and antioxidant activity, J. Mater. Sci. 53 (2018) 15837–15849.

[40] G. F Fan, Z. Yu, G.J.R.M Tang Dai, .Z.G. Xu, Preparation of gallic acid-hydroxypropyl-beta-cyclodextrin inclusion compound and study on its effect mechanism on Escherichia coli in vitro, Mater. Express 11 (11) (2021) 655–662.

[41] N. VimalasruthI, A. Manawwer, A. Naushad, B. Suganya Bharathi, G. Vigneshkumar, S. Esakkimuthu, R. Brindha, T. Stalin, Electrospun poly (vinyl alcohol) nanofibers incorporating caffeic acid/cyclodextrins through the supramolecular assembly for antibacterial activity, Spectrochim. Acta A 249 (2021), 119308.

[42] N. Vimalasruthi, M. Murali Krishnan, T. Stalin, Electrospinning preparation and spectral characterizations of the inclusion complex of ferulic acid and γ-cyclodextrin with encapsulation into polyvinyl alcohol electrospun nanofibers, J. Mol. Struct. 1221 (2020), 128767.

[43] X. Wei, A. Mohan Raj, J. Ji, W. Wu, G. Veerakanellore, C. Yang, V. Ramamurthy, Reversal of regioselectivity during photodimerization of 2-anthracenecarboxylic acid in a water-soluble organic cavitand, Org. Lett. 21 (2019) 7868–7872.

[44] K.A. Vandera, P. Picconi, M. Valero, G. González-Gaitano, A. Woods, L.A. Clifton, M.W.A. Skoda, K.M. Rahman, R.D. Harvey, C.A. Dreiss, Antibiotic-in-cyclodextrin-in-liposomes: formulation development and interactions with model bacterial membranes, Mol. Pharm. 17 (2020) 2354–2369.

[45] F. Shen, Y. Zhang, X. Dai, H. Zhang, Y. Liu, Alkyl-substituted cucurbit[6]uril bridged β-cyclodextrin dimer mediated intramolecular FRET behavior, J. Org. Chem. 85 (2020) 6131–6136.

[46] H.A. Benesi, J.H. Hildebrand, A spectrophotometric investigation of the interaction of iodine with aromatic hydrocarbons, J. Am. Chem. Soc. 71 (1949) 2703–2707.

[47] M. Shanmugam, D. Ramesh, V. Nagalakshmi, R. Kavitha, R. Rajamohan, T. Stalin, Host–guest interaction of L-tyrosine with β-cyclodextrin, Spectrochim. Acta A 71 (2008) 125–132.

[48] T. Stalin, N. Rajendiran, Intramolecular charge transfer effects on 3-aminobenzoic acid, Chem. Phys. 322 (2006) 311.

[49] K. Sivakumar, G. Hemalatha, M. Parameswari, T. Stalin, Spectral, electrochemical and docking studies of 5-indanol: β-CD inclusion complex, Phys. Chem. Liq. 51 (2013) 567–585.

[50] X.J. Dang, M.Y. Nie, J. Tong, H.L. Li, Inclusion of the parent molecules of some drugs with β-cyclodextrin studied by electrochemical and spectrometric methods, J. Electroanal. Chem. 448 (1998) 61.

[51] K. Srinivasan, T. Stalin, A. Shanmugapriya, K. Sivakumar, Spectroscopic and electrochemical studies on the interaction of an inclusion complex of β-cyclodextrin with 2,6-dinitrophenol in aqueous and solid phases, J. Mol. Struct. 1036 (2013) 494–504.

[52] G. Narayanan, R. Boy, B.S. Gupta, A.E. Tonelli, Analytical techniques for characterizing cyclodextrins and their inclusion complexes with large and small molecular weight guest molecules, Polym. Test. 62 (2017) 402–439.

[53] P. Mura, Analytical techniques for characterization of cyclodextrin complexes in the solid state: a review, J. Pharm. Biomed. Anal. 113 (2015) 226–238.

[54] B. Rajbanshi, S. Saha, K. Das, B. Barman, S. Sengupta, A. Bhattacharjee, M. Roy, Study to probe subsistence of host-guest inclusion complexes of α and β-cyclodextrins with biologically potent drugs for safety regulatory dischargement, Sci. Rep. 8 (2018) 13031.

[55] R. Periasamy, S. Kothainayaki, R. Rajamohan, K. Sivakumar, Spectral investigation and characterization of host–guest inclusion complex of 4,4′-methylene-bis(2-chloroaniline) with beta-cyclodextrin, Carb. Pol. 114 (2014) 558–566.
[56] R. Periasamy, R. Rajamohan, S. Kothainayaki, K. Sivakumar, Spectral investigation and structural characterization of Dibenzalacetone: β-Cyclodextrin inclusion complex, J. Mol. Struct. 1068 (2014) 155–163.
[57] C.I. Nkanga, R.W.M. Krause, Encapsulation of isoniazidconjugated phthalocyanine-incyclodextrin-In-liposomes using heating method, Sci. Rep. 9 (2019) 11485.
[58] N. Amanokura, M. Kaneko, T. Sahara, R. Sato, Curing behavior of epoxy resin initiated by amine-containing inclusion complexes, Pol. J. 39 (2007) 845–852.
[59] Q. Geng, T. Li, X. Wang, W. Chu, M. Cai, J. Xie, H. Ni, The mechanism of bensulfuronmethyl complexation with β-cyclodextrin and 2-hydroxypropyl-β-cyclodextrin and efect on soil adsorption and bio-activity, Sci. Rep. 9 (2019) 1882.
[60] J.S. Choi, J.C. Byeon, J.S. Park, Naftopidil-fumaric acid interaction in a solid dispersion system: improving the dissolution rate and oral absorption of naftopidil in rats, Mat. Sci. Eng. C 95 (2019) 264–274.
[61] J. Jumina, W. Lavendi, T. Singgih, S. Triono, Y. Kurniawan, M. Koketsu, Preparation of monoacylglycerol derivatives from indonesian edible oil and their antimicrobial assay against staphylococcus aureus and Escherichia coli, Sci. Rep. 9 (2019) 10941.